引用格式：WU Tiesheng, YANG Zuning, ZHANG Huixia, et al. Refractive Index Sensing Characteristics of D-shaped High Birefringent Photonic Crystal Fiber[J]. Acta Photonica Sinica, 2022, 51(3):0306003
伍铁生,杨祖宁,张慧仙,等.D型高双折射光子晶体光纤的折射率传感特性研究[J].光子学报,2022,51(3):0306003

D型高双折射光子晶体光纤的折射率传感特性研究

伍铁生[1,2,3],杨祖宁[1],张慧仙[1],刘智慧[1],杨丹[1],钟旭[1],刘岩[1],刘锐[1]
(1 桂林电子科技大学 信息与通信学院 广西无线宽带通信与信号处理重点实验室,广西 桂林 541004)
(2 深圳大学 光电工程学院 光电子器件与系统教育部重点实验室,广东 深圳 518060)
(3 深圳大学 光电工程学院 广东省光纤传感技术粤港联合研究中心,广东 深圳 518060)

摘 要:基于表面等离子体共振(SPR)原理,分析了D型高双折射光子晶体光纤(HB-PCF)的折射率传感特性。模拟研究了抛磨角度对双折射、折射率传感灵敏度的影响。仿真结果表明:当抛磨面离纤芯的高度小于1.5倍占空比时,抛磨面离纤芯越近,双折射越小;随着抛磨角度的增加,双折射先增加后减小,折射率传感灵敏度随之减小;当抛磨角度为0°且折射率范围在1.330~1.390时,D型HB-PCF的平均折射率灵敏度高达2 833.33 nm/RIU。此外,制备了一种D型高双折射率光子晶体光纤SPR传感器,实验测得其折射率灵敏度约为1 711.83 nm/RIU。D型HB-PCF SPR传感器可应用于生物、化学和环境监测等领域。

关键词:光子晶体光纤;表面等离子体共振;折射率;传感器;侧边抛磨
中图分类号:TN253 **文献标识码**:A **doi**:10.3788/gzxb20225103.0306003

0 引言

表面等离子共振(Surface Plasmon Resonance,SPR)是一种物理现象,当入射光的频率与波数与金属表面振动的自由电子(即等离子)频率一致时,则金属表面的电子(即等离子)吸收光能发生共振,其共振波长随贵金属表面折射率变化而变化,而折射率的变化又与贵金属表面结合的分子质量密切相关[1-7]。因此SPR在生命科学、医疗检测、药物筛选、环境监测、食品检测等领域具有广泛的应用需求[8-11]。1902年,美国著名物理学家WOOD R W[12]首次参观到了SPR现象,1941年[13],科学家解释了SPR现象的物理原理。1968年,KRETSCHMANN E[14]提出了两种激发SPR的棱形结构,为SPR传感技术的应用奠定了实验基础。1983年,KULLMAN E[15]将SPR用于IgG与其抗原的反应测定并取得了成功。到了1993年,JORGENSON R等[16]提出了SPR光纤传感器,为SPR技术更加广泛的应用开启了新的乐章。在过去的二十年中,为提高光纤SPR传感器的性能,人们致力于调整和优化基于光纤SPR传感器的设计。为了提高灵敏度和降低谐振峰的窄半峰全宽,人们用单模光纤替代多模光纤作为传感元件。随后出现的光纤SPR传感器结构,为了允许沉积薄金属(主要是Au或Ag)层,光纤的包层被移除(传感区域),该层支持SPR的激发及其与光纤的光波导模式的相互作用。这些结构包括修饰光纤端面[17]、锥形光纤[18]、D形光纤[19]、光纤光栅[20]和光子晶体光纤[21]。

如今,基于微结构光纤的SPR传感器因其在生化传感领域具有广泛的应用前景而越来越受欢迎。然

基金项目:国家自然科学基金(No.61805051),广西自然科学基金(Nos.2018JJB170035,2018AD19071,2019GXNSFFA245002,2020JJA170047),广西无线宽带通信与信号处理重点实验室主任基金(Nos.GXKL06190118,GXKL0616102,GXKL06180203,GXKL06180104)
第一作者(通讯作者):伍铁生(1983—),男,副教授,博士,主要研究方向为光电子器件、微波光子技术、光纤传感技术、新型二维材料等。Email:tieshengw@163.com
收稿日期:2021-09-26;**录用日期**:2021-11-04

而，许多研究人员遇到的困难是在设计微结构光纤SPR传感器时很难做到实现等离子体共振模式与纤芯模式的完全匹配及空气孔内分析液难以清理。作为创新的解决方案，LUAN Nannan等[22]提出了一种基于微结构光纤SPR传感器，该结构以两种特殊设计为特色。特色一是结构设计为D形空心光纤，可以降低类高斯纤芯模式的折射率，以匹配等离子模式的折射率。另一个新颖之处在于沉积分析物的方法，即将分析物直接沉积在D形平面上，而不是填充纤芯。通过这种方法，获得了令人满意的光谱灵敏度(2 900 nm/RIU)。此后，基于镀膜D型光子晶体光纤，CHEN Hailiang等[23]设计了一种超宽带宽偏振滤波器，该结构的一个好处是它有助于在光纤波导模式和表面等离子体激元(Surface Plasmon Polaritons，SPPs)模式之间产生多重共振。类似的，TAN Zhixin等[24]对深度抛磨的全固态光子晶体光纤SPR传感器进行了数值研究，利用相位调制，采用相位询问法，计算得到灵敏度为9.09×104°/RIU，理论值高于常规的波长检测灵敏度。值得注意的是，XIE Qingli等[25]实验研究了侧边抛磨深度和传感层厚度对D形光子晶体光纤表面等离子体共振传感器性能的影响，发现传感灵敏度随着传感层厚度的增加而增加。但当侧抛深度达到一定范围时，传感器灵敏度略有下降，实验测得在1.40～1.42的折射率范围内，传感器最高灵敏度可达7 381.0 nm/RIU。事实上，对于光纤SPR传感器，测量的分析液折射率越高，灵敏度越大。此外，TONG Kai等[26]提出了一种基于TiO_2薄膜增强的PCF-SPR的生物传感器，折射率灵敏度可达4 200 nm/RIU。CHEN Qianghua等[27]提出了一种基于棱镜结构的具有四层介质的光纤表面等离子体共振的传感器，用于检测溶液折射率变化。GANDHI M A等[28]以D型PDF为基质，设计了三种金属沉积方案，实现了高灵敏度传感，可用于生物、化学检测。

目前基于光子晶体光纤SPR传感器的报道，主要是以理论模型的建立和数值仿真为主，实验制备基于光子晶体光纤 SPR传感器较为困难。本文提出了一种D型高双折射光子晶体光纤(High Birefringence Photonic Crystal Fiber，HB-PCF)传感器。理论上，采用有限元(Finite Element Method，FEM)数值分析，仿真分析了抛磨深度、抛磨角度对双折射的影响，研究了折射率传感灵敏度与抛磨角度的关系。实验上，制备了D型PCF-SPR传感器样品，分别实现了对不同折射率匹配液和不同浓度葡萄糖溶液的检测。

1 结构模型与仿真分析

基于D型高双折射光子晶体光纤的SPR传感器模型结构示意图如图1所示。根据实验采用的高双折射光子晶体光纤，仿真模型的光子晶体光纤由五层空气孔排列组成，包层中第一层含有两个较大的空气孔，其中晶格间距Λ为4.4 μm，小空气孔直径d_1为2.2 μm，大空气孔直径d_2为4.5 μm，抛磨深度为h，即光子晶体光纤纤芯到抛磨表面的距离，高双折射光子晶体光纤慢轴与抛磨面之间的夹角定义为抛磨方向θ。金薄膜涂覆在光纤平坦的抛磨面上，以便于和待测物体接触。根据以往的理论和实验研究，把金膜的厚度(t)设置为45 nm。仿真中用到的光子晶体光纤背景材料折射率和金的折射率由线性插值的实验数据给出。为了得到侧边抛磨高双折射光子晶体光纤的波导模式，采用有限元法商用软件COMSOL Multiphysics并设置完美匹配层边界条件来进行仿真，分析物的折射率设置为1.330到1.400范围内。波长灵敏度定义为$S_\lambda=\Delta\lambda_{res}/\Delta n_a$，其中$\lambda_{res}$是D型光子晶体光纤传感器的等离子共振波长，$n_a$是分析物折射率。在波导光学领域，限制损耗由等式(1)计算得出[29]。

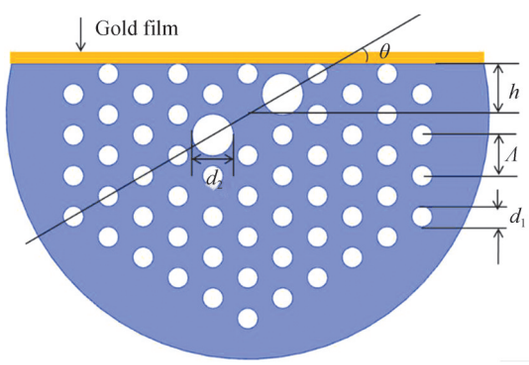

图1 基于D型高双折射光子晶体光纤的SPR传感器模型结构示意图

Fig. 1 Schematic diagram of the SPR sensor based on D-shaped high birefringence photonic crystal fiber

$$\alpha = 8.686 \cdot k_0 \, \mathrm{Im}[n_{\mathrm{eff}}] (\mathrm{dB/m}) \tag{1}$$

式中，$k_0 = 2\pi/\lambda$ 为传播常数，单位为 m。

首先研究抛磨对 PCF 双折射效应的影响。抛磨深度对双折射的影响如图 2(a)所示，抛磨方向设置为 0°，光波长分别设置为 500 nm、1 000 nm、1 500 nm，由图 2 可知，当抛磨面离纤芯的距离大于 1.5 倍空占比时，侧边抛磨光纤几乎不对双折射产生影响，在 1～1.5 倍空占比之间，影响较小，当抛磨面离纤芯距离小于 1 倍空占比时，抛磨面离纤芯越近，双折射越小，同一抛磨深度，波长越大，双折射也越大。图 2(b)是抛磨角度对双折射的影响，很显然，抛磨方向对双折射的影响较小，在波长较小时，其影响可以负略不计。

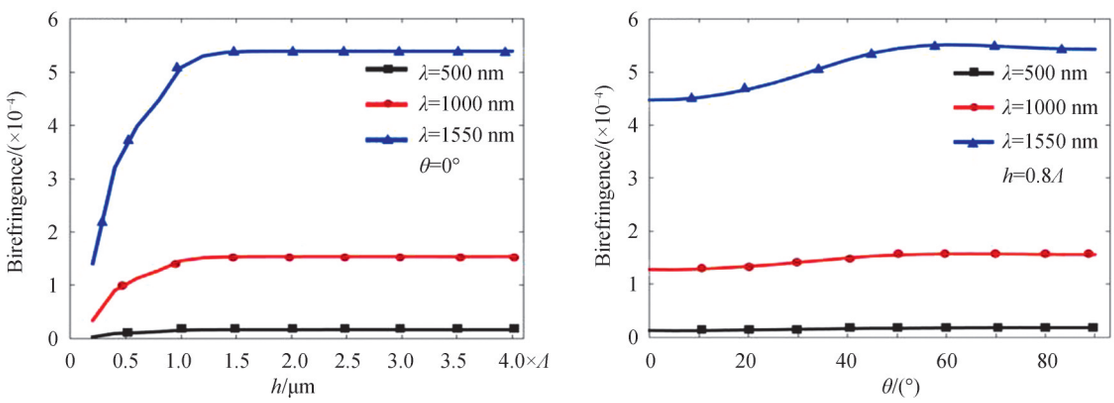

(a) Effect of polishing height on birefringence　　(b) Effect of polishing angle on birefringence

图 2　抛磨高度和抛磨角度对光子晶体光纤双折射的影响

Fig. 2　The influence of polishing height and polishing angle on the birefringence of photonic crystal fiber

图 3(a)给出了纤芯 TM 波导模有效折射率、SPPs 有限折射率及纤芯 TM 波导模的损耗与波长的关系。其中，金纳米薄膜表面待测物折射率设置为 1.33，抛磨角度 θ 为 0°、抛磨深度 h 为 0.8Λ，d_1 为 4.5 μm，d_2 为 2.2 μm，Λ 为 4.4 μm。由图 3(a)可知，纤芯模式有效折射率和 SPPs 有限折射率随着波长的增加而线性减小，在波长约为 595 nm 处，两者发生相交即纤芯 TM 模式有效折射率和 SPPs 有限折射率相等，满足相位匹配条件下，此时将发生表面等离子体共振效应，使得纤芯能量大部分转移到金纳米薄膜层附近，表现为纤芯导模在此波长有一个损耗峰。为进一步说明该物理现象，比较了波长在 500 nm 和 595 nm 处纤芯导模和等离子体模式的的电场分布，图 3(b)为波长 λ 在 500 nm 处的纤芯 TE 模，图 3(c)为波长 λ 在 500 nm 处的纤芯 TM 模，图

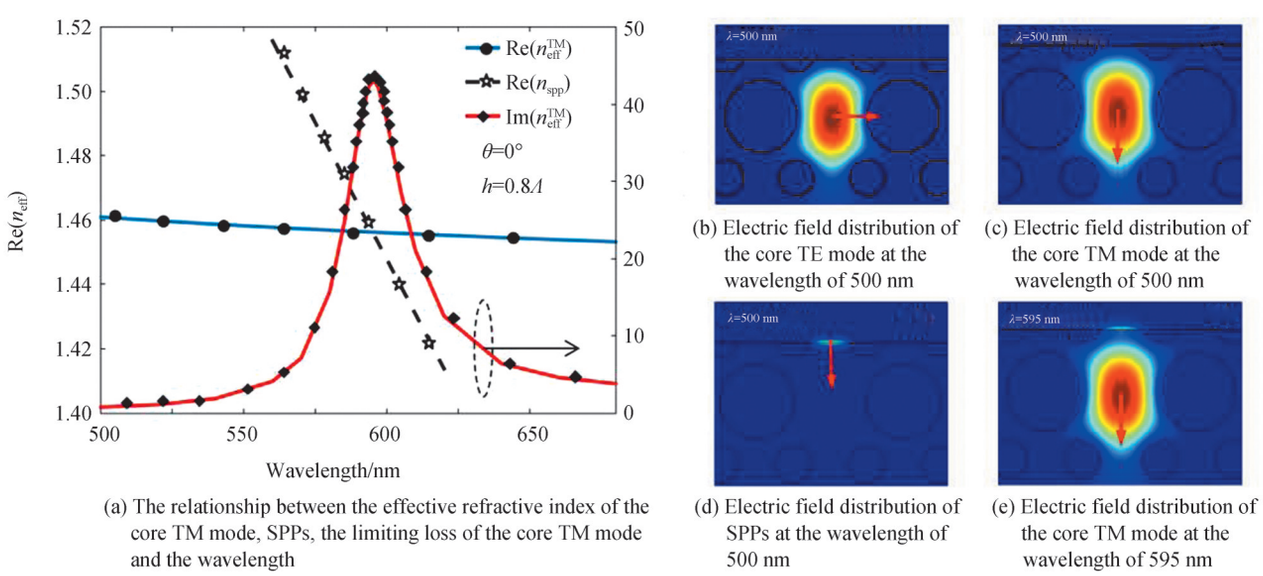

(a) The relationship between the effective refractive index of the core TM mode, SPPs, the limiting loss of the core TM mode and the wavelength

(b) Electric field distribution of the core TE mode at the wavelength of 500 nm

(c) Electric field distribution of the core TM mode at the wavelength of 500 nm

(d) Electric field distribution of SPPs at the wavelength of 500 nm

(e) Electric field distribution of the core TM mode at the wavelength of 595 nm

图 3　模式的有效折射率及模场分布

Fig. 3　Effective refractive index and mode field distribution of the mode

3(d)为波长λ在500 nm处的等离子体模，图3(e)为波长λ在595 nm处即达到相位匹配时同时可观察到纤芯导模和等离子体模式。很显然在该波长纤芯TM模和等离子模式发生了显著的耦合。

研究D型高双折射光子晶体光纤的SPR传感特性。其传感原理为：由于SPR对环境折射率变化非常灵敏，当环境折射率变化时，纤芯TM模式损耗谱峰值会发生漂移，根据损耗光谱中的峰值波长和待测物折射率之间的关系，利用波长询问法，通过测量损耗光谱的峰值波长来待测物折射率。图4(a)展示了D型高双折射光子晶体光纤的抛磨角度θ为0°、抛磨深度为0.2Λ，d_1为4.5 μm，d_2为2.2 μm，Λ为4.4 μm时，待测物折射率n分别为1.330、1.340、1.350时纤芯TM模的损耗谱。随着待测分析物折射率的增加，损耗光谱的峰值波长呈现红移，耦合强度也相应地增加。图4(b)是折射率从1.330变化到1.400时，待测分析物折射率和损耗谱峰值波长、峰值损耗大小的关系，由图4(b)可知，损耗谱的峰值损耗、峰值波长(谐振波长)随着分析液折射率的增加而增大。根据折射率灵敏度的定义，在1.330～1.400折射率范围，计算可得D型HB-PCF的平均折射率灵敏度高达3 457.14 nm/RIU，该结果优于D型单模光纤及D型全内反射型光子晶体光纤SPR传感器的性能[29-30]。

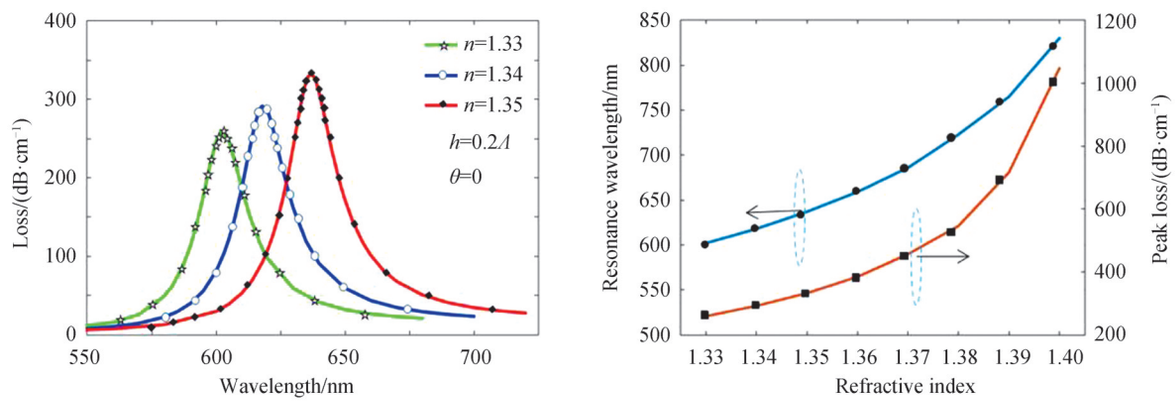

(a) Loss spectral curves corresponding to different refractive index of analyte

(b) The relationship between refractive index and resonance wavelength and peak loss

图4 折射率传感理论分析

Fig. 4 Refractive index sensing theory analysis

根据前面的理论和实验研究[29]，光纤的抛磨深度会影响纤芯模式和等离子体模式的耦合强度，但不会影响D型光纤SPR传感器的灵敏度，因此只对抛磨角度对D型的HB-PCF SPR传感器的灵敏度进行分析，如图5(a)所示。图5(a)是抛磨深度为0.6Λ，待测分析物折射率n分别为1.330和1.400，不同抛磨角度下的D型HB-PCF的损耗谱。由图5(a)可知，其他参数不变情况下，抛磨角度的变化会影响谐振波长的位置。随

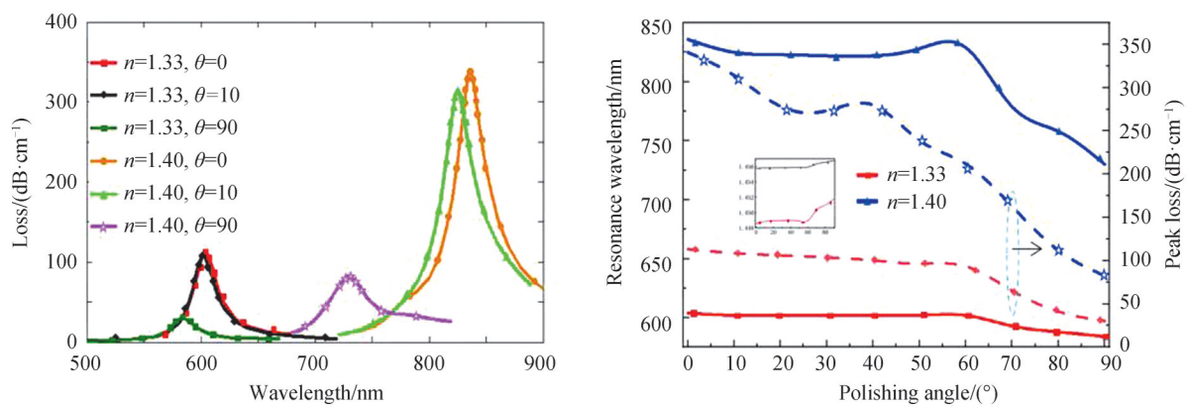

(a) Loss spectral curves of different refractive indexes under different polishing angles

(b) Relation between polishing angle and resonance wavelength

图5 抛磨角度对D型高双折射PCF光传输特性影响

Fig. 5 Effect of polishing angle on the optical transmission characteristics of D-type highly birefringent PCF

着抛磨角度的增大，损耗谱的峰值损耗降低，且损耗峰值波长发生蓝移。图5(b)是谐振波长、损耗谱峰值与抛磨角度的关系。由图5(a)可知，抛磨角度从0°逐渐增加到60°时，谐振波长漂移变化缓慢，但是在60°到90°的范围，该过程随着抛磨角度的增加，谐振波长发生显著的漂移，分析液折射率越高，谐振波长受到的影响越大。

2 实验与讨论

实验上，制备了D型高双折射光子晶体光纤SPR传感器样品并进行了测试。实验选择由长飞光纤光缆股份有限公司生产的保偏光子晶体光纤(型号：PC1013-A)。图6为光子晶体光侧边抛磨示意图。首先，在两个单模光纤之间熔接一段10 nm长的PCF，然后熔接的光纤由一对光纤夹持器夹住固定。在这个光纤抛磨系统中，砂轮固定在可以沿着x、y、z方向移动的3D机械平台上。抛磨长度和抛磨深度可通过计算机程序精确设置和操作。为了加快抛磨的速度，使用小重量的砝码挂在光纤上来拉直光子晶体光纤并提供合适的抛磨力度。在机械轮上固定砂纸用于抛磨光纤。实时监测抛磨过程用的宽带光源(BBS)波长范围为1 250 nm到1 650 nm，光谱分析仪型号为OSA，Yokogawa AQ6370C。用沾酒精的无尘纸轻轻清洁光子晶体光纤抛磨表面以去除残留的二氧化硅微尘。当抛磨面接近光子晶体光纤的纤芯时，即刻停止抛磨。

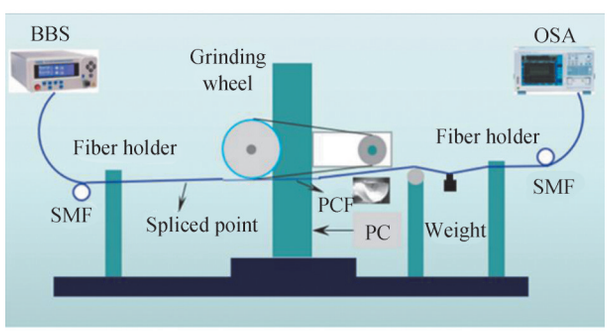

图6 侧边抛磨光子晶体光纤系统示意图
Fig. 6 Photonic crystal fiber side-polised system

在对光子晶体光纤完成抛磨后，通过光纤磁控溅射涂层机(LN-JS2，沈阳真空技术研究所)在抛磨好的光子晶体光纤平坦的表面上沉积45 nm厚度的金薄膜。最后，即可完成侧边抛磨的PCF-SPR传感器的制备工作，抛磨长度为7 mm，抛磨深度为0.88 μm，所获D型高双折射光子晶体光纤在显微镜下观察到的实物如图7所示。

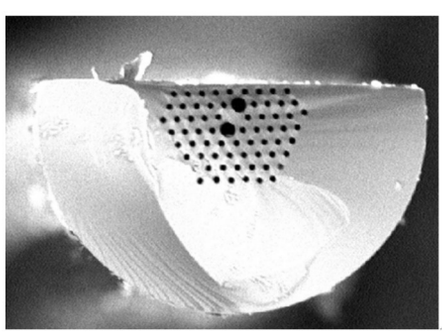

图7 D型高双折射光子晶体光纤横截面示意图
Fig. 7 Cross-section of D-shaped high birefringence photonic crystal fiber

图8为搭建的SPR传感器实验测试装置。在此传感测量系统中，光源采取具有450 nm至1 100 nm宽带的卤钨素灯(LS-300，Ocean Optics Inc)。光谱仪采用一种微型光谱仪(USB6500，Ocean Optics Inc)，其测量范围为200 nm至1 100 nm。白光通过单模光纤传输到PCF-SPR传感器中，并受D型平面上折射率匹配液体的调制。最后，在室温下的调制信号由光谱仪记录并通过笔记本电脑的USB端口处理。实验中，需要在

每个后续测量之前用酒精反复清洗传感器以确保感测敏感区域的清洁。

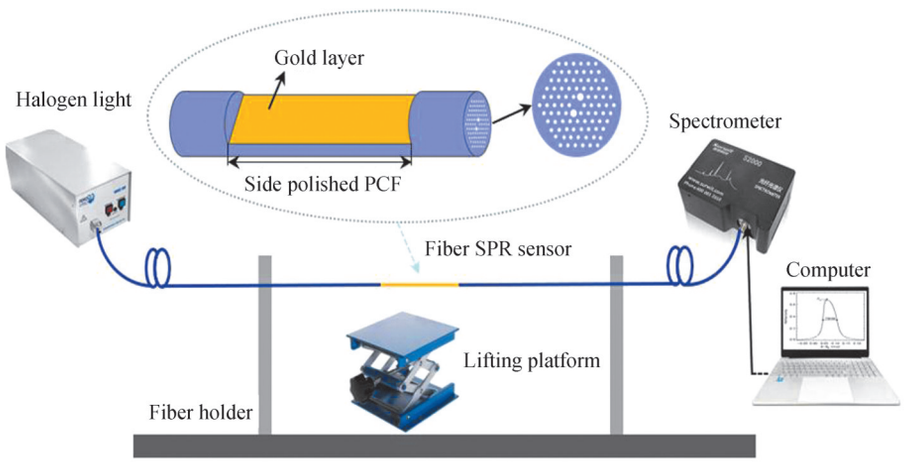

图8 实时在线测量系统的示意图

Fig. 8 Schematic diagram of real-time online measurement system

D型高双折射光子晶体光纤的折射率传感测试结果如图9(a)所示。归一化透射光谱根据传感器浸入液体时的透射率与传感器暴露在空气中的透射率之比来计算。作为电磁场从纤芯TM模耦合到金膜附近谐振波长处SPP模式的结果,当传感器浸入每种折射率匹配液时,传输谱中会出现明显的吸收峰。随着匹配液折射率的增加,传输谱的凹点波长会出现红移,且凹点深度会随着匹配液折射率的增加而增大。图9(b)是谐振波长和分析液折射率变化之间的非线性关系。随着匹配液折射率的增加,D型高双折射光子晶体光纤的折射率灵敏度逐渐增大。计算可得其在1.330~1.390折射率范围的平均折射率灵敏度约为1 711.83 nm/RIU。由图4(b)可知,在该折射率范围,其折射率灵敏度理论值为2 833.33 nm/RIU。理论和实验上的灵敏度值相差较大,主要原因有:1)抛磨面不平整(空气孔带来的缺陷),使得抛磨过程中产生的碎屑不易完全清除,这会影响传感的性能;2)完成D型光纤样品制备后,没有及时对光纤做镀膜处理,D型光纤长时间暴露在空气中,空气中的尘埃附着在D型面会进一步影响器件性能;3)尽管在每次测试之前均会反复用乙醇清洗传感器,但是难以把留在PCF空气孔中折射率匹配液完全清除,从而影响后续测量结果的准确性,例如,第一次测试折射率1.33,通过酒精清洗,滴1.34的光纤匹配液,由于前面的液体残留,真实值很难做到1.34,而计算依旧按照1.34计算;4)理论的最大值是在抛磨平面与两个大空气孔连线平行条件下获得的,理论仿真已表明其灵敏度与抛磨的方向有关,测试样品的抛磨面并不与两个大空气孔的连线平行。

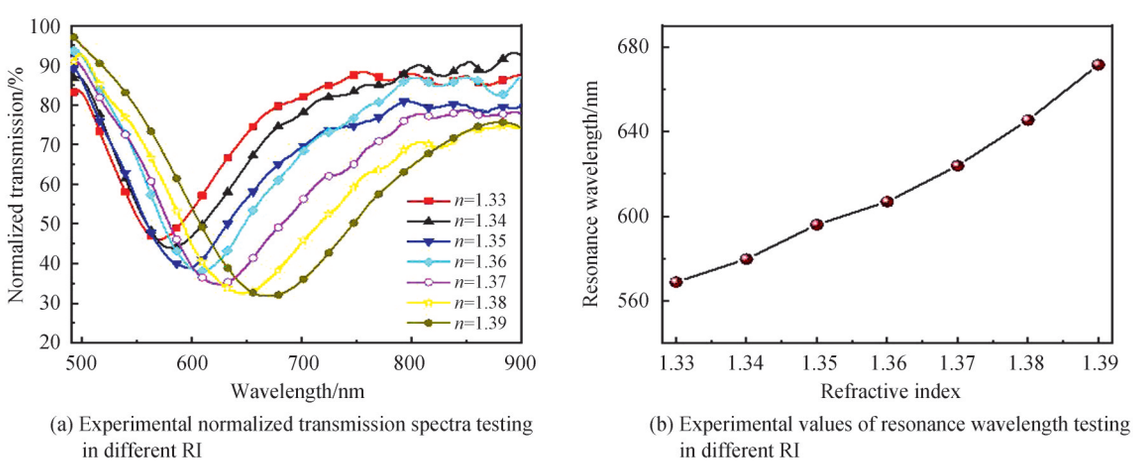

(a) Experimental normalized transmission spectra testing in different RI

(b) Experimental values of resonance wavelength testing in different RI

图9 折射率传感实验分析

Fig. 9 Experimental analysis of refractive index sensing

进一步用该D型高双折射光子晶体光纤SPR传感器测试葡萄糖溶解的浓度，实验结果如图10(a)所示。葡萄糖溶液浓度以2 g/dL的步长，从0 g/dL增加至10 g/dL，由图10(a)可知随着葡糖糖浓度的增加，D型高双折射光子晶体光纤SPR传感器的传输谱凹点峰值波长会发生红移。在0g/dL的葡萄糖溶液中，SPR共振波长出现在578.96 nm处，而当葡萄糖溶液浓度为10 g/dL时，SPR共振波长漂移到587.49 nm处。图10(b)给出了葡萄糖浓度与传输谱凹点峰值波长的关系，经计算，其平均灵敏度为1.89 nm/(g/dL)。

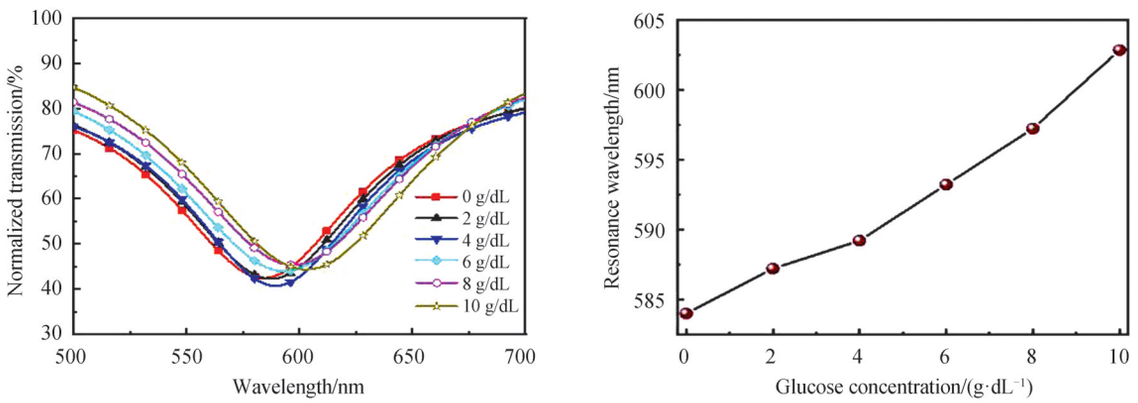

(a) Experimental normalized transmission spectra testing in different glucose concentrations

(b) The relationship between glucose concentration and resonance wavelength

图10 葡萄糖浓度检测分析

Fig. 10 Glucose concentration detection analysis

3 结论

基于SPR原理，本文数值仿真和实验研究了D型HB-PCF的折射率传感特性。金膜和分析液被沉积在HB-PCF抛磨的表面。通过有限元法建模仿真，研究了抛磨角度对双折射、折射率传感灵敏度的影响。仿真结果表明：高双折射光子晶体光纤的双折射效应受抛磨深度的调制；而折射率灵敏度与抛磨角度密切相关；当抛磨角度为0°且折射率范围在1.330～1.400时，D型HB-PCF的平均折射率灵敏度可达3 457.14 nm/RIU。实验制备了D型HB-PCF SPR传感器，并测试了其折射率传感。D型高双折射光子晶体光纤SPR传感器可以实现在生物、化学和环境监测等领域的应用。

参考文献

[1] JORGENSON R, YEE S. A fiber-optic chemical sensor based on surface plasmon resonance[J]. Sensors and Actuators B Chemical, 1993, 12(3): 213-220.

[2] LI Jiahuan, PEI Li, WANG Jianshuai, et al. Dual parametric temperature and magnetic field sensor based on surface plasmon resonance of photonic crystal fiber[J]. Chinese Journal of Lasers, 2019, 46(2): 0210002.
李佳欢, 裴丽, 王建帅, 等. 基于光子晶体光纤表面等离子体共振的温度和磁场双参量传感器[J]. 中国激光, 2019, 46(2): 0210002.

[3] SUZUKI H, SUGIMOTO M, MATSUI Y, et al. Effects of gold film thickness on spectrum profile and sensitivity of a multimode-optical-fiber SPR sensor[J]. Sensors and Actuators B Chemical, 2008, 132(1): 26-33.

[4] LIU Zhihai, WEI Yong, ZHANG Yu, et al. Reflective-distributed SPR sensor based on twin-core fiber[J]. Optics Communications, 2016, 366: 107-111.

[5] CHIU M, WANG S, CHANG R . D-type fiber biosensor based on surface-plasmon resonance technology and heterodyne interferometry[J]. Optics Letters, 2005, 30(3): 233-235.

[6] SENTHILNATHAN K, PATNAIK, et al. Graphene-based conducting metal oxide coated D-shaped optical fiber SPR sensor[J]. IEEE Photonics Technology Letters, 2015, 27(23): 2437-2440.

[7] HE Yuejing. Novel D-shape LSPR fiber sensor based on nano-metal strips[J]. Optics Express, 2013, 21(20): 23498-23510.

[8] YANG Yang, ZHU Xiaotong, YAN Liangjun, et al. High-precision curvature sensing technology based on side-surfaced single-mode fibers[J]. Acta Optica Sinica, 2020, 40(14): 1406004.
杨洋, 朱肖彤, 闫良俊, 等. 基于侧边粗抛磨单模光纤的高精度曲率传感技术研究[J]. 光学学报, 2020, 40(14): 1406004.

[9] GAO Di, GUAN Chunying, WEN Yaowu, et al. Multi-hole fiber based surface plasmon resonance sensor operated at near-infrared wavelengths[J]. Optics Communications, 2014, 313:94-98.
[10] LIU Yundong, CHEN Hailiang, GUO Ying, et al. Ultra-high sensitivity plasmonic sensor based on D-shaped Photonic crystal fiber with offset-core[J]. Optik-International Journal for Light and Electron Optics, 2020, 221:165309.
[11] CHEN Hailiang, LI Shuguang, AN Guowen, et al. Polarization splitter based on D-shaped dual-core photonic crystal fibers with gold film[J]. Plasmonics, 2015, 10(1):57-61.
[12] WOOD R W. On a remarkable case of uneven distribution of light in a diffraction grating spectrum[J]. Proceedings of the Physical Society of London, 1902, 18(1): 269-275.
[13] FANO M D. Mechanism of the origin of X-ray induced notch deficiencies in drosophila melanogaster[J]. Proceedings of the National Academy of Sciences of the United States of America, 1941, 27(1): 24-31.
[14] KRETSCHMANN E, RAETHER H. Radiative decay of non radiative surface plasmons excited by light[J]. Zeitschrift Für Naturforschung A, 1968, 23(12): 2135-2136.
[15] KULLMAN E, BORCH K, LIEDBERG G, et al. Endoscopic sphincterotomy in the treatment of choledocholithiasis and ampullar stenosis. Experience with 202 patients[J]. Acta Chirurgica Scandinavica, 1985, 151(7): 619-624.
[16] JORGENSON R, YEE S. A fiber-optic chemical sensor based on surface plasmon resonance[J]. Sensors and Actuators B: Chemical, 1993, 12(3): 213-220.
[17] ZHANG Yu, WEI Yong, LIU Zhihai, et al. Twin-core fiber SPR sensor[J]. Optics Letters, 2015, 40(12):2826-2829.
[18] MONZON H, VILLATORO J. High-resolution refractive index sensing by means of a multiple-peak surface plasmon resonance optical fiber sensor[J]. Sensors & Actuators B Chemical, 2006, 115(1):227-231.
[19] TIAN Ming, LU Ping, CHEN Li, et al. All-solid D-shaped photonic fiber sensor based on surface plasmon resonance [J]. Optics Communications, 2012, 285(6): 1550-1554.
[20] PAKOVA, BARBORA, HOMOLA, et al. Theoretical analysis of a fiber optic surface plasmon resonance sensor utilizing a Bragg grating[J]. Optics Express, 2009, 17(25): 23254.
[21] LI Jing, DENG Zequn, ZHAO Yong. Photonic crystal fiber based surface plasmon resonance chemical sensors [J]. Sensors and Actuators B: Chemical, 2014, 202: 557-567.
[22] LUAN Nannan, WANG Ran, LV Wenhua, et al. Surface plasmon resonance sensor based on D-shaped microstructured optical fiber with hollow core[J]. Optics Express, 2015, 23(7): 8576-8582.
[23] CHEN Hailiang, LI Shuguang, AN Guowen, et al. Polarization splitter based on d-shaped dual-core photonic crystal fibers with gold film[J]. Plasmonics, 2015, 10(1): 57-61.
[24] TAN Zhixin, HAO Xin, SHAO Yonghong, et al. Phase modulation and structural effects in a D-shaped all-solid photonic crystal fiber surface plasmon resonance sensor[J]. Optics Express, 2014, 22(12): 15049-15063.
[25] XIE Qingli, CHEN Yuzhi, LI Xuejin, et al. Characteristics of D-shaped photonic crystal fiber surface plasmon resonance sensors with different side-polished lengths[J]. Applied Optics, 2017, 56(5): 1550-1555.
[26] TONG Kai, DANG Peng, WANG Meiting, et al. Modeling analysis of the sensitivity of surface plasmon resonance biosensors using TiO_2 thin film enhanced photonic crystal fibers[J]. Chinese Journal of Lasers, 2018, 45(6): 0610002.
童凯,党鹏,汪梅婷,等. 采用TiO_2薄膜增强光子晶体光纤表面等离子体共振生物传感器灵敏度的建模分析[J]. 中国激光, 2018, 45(6): 0610002.
[27] CHEN Qianghua, HAN Wenyuan, KONG Xiangyue. Detection of refractive index changes in solutions based on plasmon resonance on optical fiber surfaces[J]. Chinese Journal of Lasers, 2020, 47(8): 0804003.
陈强华,韩文远,孔祥悦,等. 基于光纤表面等离子体共振检测溶液折射率变化[J]. 中国激光, 2020, 47(8): 0804003.
[28] GANDHI M, SENTHILNATHAN K, BABU P, et al. Highly sensitive localized surface plasmon polariton based D-type twin-hole photonic crystal fiber microbiosensor: enhanced scheme for SERS reinforcement[J]. Sensors, 2020, 20 (18): 5248.
[29] WU Tiesheng, SHAO Yu, WANG Ying, et al. Surface plasmon resonance biosensor based on gold-coated side-polished hexagonal structure photonic crystal fiber [J]. Optics Experss, 2017, 25(17): 20313-20322.
[30] HEMANT K, UMANG R, BIPIN K, et al. Investigations on the highly sensitive metal-coated broad range D-shaped optical fiber refractive index sensor [J]. Plasmonics, 2021, 23(7): 8329-8337.

Refractive Index Sensing Characteristics of D-shaped High Birefringent Photonic Crystal Fiber

WU Tiesheng[1,2,3], YANG Zuning[1], ZHANG Huixia[1], LIU Zhihui[1], YANG Dan[1], ZHONG Xu[1], LIU Yan[1], LIU Rui[1]

(1 *Guangxi Key Laboratory of Wireless Broadband Communication and Signal Processing, College of Information and Communication, Guilin University of ELectronic Technology, Guilin, Guangxi* 541004, *China*)

(2 *Key Laboratory of Optoelectronic Devices and Systems of Ministry of Education, College of Optoelectronic Engineering, Shenzhen University, Shenzhen, Guangdong* 518060, *China*)

(3 *Guangdong and Hong Kong Joint Research Centre for Optical Fiber Sensors, College of Optoelectronic Engineering, Shenzhen University, Shenzhen, Guangdong* 518060, *China*)

Abstract: Surface Plasmon Resonance (SPR) is a physical phenomenon, when the frequency and wave number of incident light coincide with the frequency of free electrons vibrating on the metal surface, then the electrons (i.e., plasma) on the metal surface absorb light energy and resonate, and its resonance wavelength changes with the refractive index of the precious metal surface, so SPR has a wide range of application needs in medical detection, environmental monitoring and other fields. Based on the principle of SPR, this work investigates the refractive index sensing characteristics of D-type highly birefringent photonic crystal fibers in detail. The current reports on PCF SPR sensors are mainly based on the establishment of theoretical models and numerical simulations. It is difficult to experimentally prepare PCF SPR sensors. According to the high birefringence photonic crystal fiber used in the experiment, the photonic crystal fiber of the simulation model is composed of five layers of air holes. The first layer of the cladding contains 2.2 μm, the diameter of the large air hole is 4.5 μm, and the polishing depth is represented by h, that is, the distance from the core of the photonic crystal fiber to the polishing surface, and the angle between the slow axis of the high birefringence photonic crystal fiber and the polishing surface is defined as the polishing direction θ. The gold film is coated on the flat polishing surface of the optical fiber to facilitate contact with the object to be measured. According to previous theoretical and experimental research, we set the thickness (t) of the gold film to 45 nm. The refractive index of the photonic crystal fiber background material and the refractive index of gold used in the simulation are given by the experimental data of linear interpolation. In order to obtain the waveguide mode of the side-polished high-birefringent photonic crystal fiber, this paper uses the finite element method commercial software COMSOL Multiphysics and sets the boundary conditions of the perfect matching layer for simulation. The refractive index of the analyte is set in the range of 1.330 to 1.400. Through finite element method modeling and simulation, the influence of polishing angle on the sensitivity of birefringence and refractive index sensing are studied in this paper. The simulation results show that when the height of the polishing surface from the fiber core is less than 1.5 times the duty cycle, the closer the polishing surface is to the core, the smaller the birefringence. As the polishing angle increases, the birefringence first increases and then decreases, and the refractive index sensing sensitivity decreases accordingly. When the polishing angle is 0 degrees and the refractive index ranges from 1.330 to 1.400, the average refractive index sensitivity of the device is as high as 3 457.14 nm/RIU. In addition, we have prepared a D-type high birefringence photonic crystal fiber SPR sensor. There is a big difference between the theoretical and experimental sensitivity values. The main reasons are: 1) The polishing surface is uneven (defects caused by air holes), which makes it difficult to completely remove the debris generated during the polishing process, which will affect the sensing performance. Performance; 2) After preparing the D-type fiber sample, the fiber is not coated in time. The D-type fiber is exposed to the air for a long time, and the dust in the air will further affect the performance of the device; 3) Although every time Before the test, the sensor will be cleaned repeatedly with ethanol, but it is difficult to completely remove the refractive index matching liquid left in the PCF air hole, which will affect the accuracy of the subsequent measurement results. For example, we tested the refractive index of 1.33 for the first time and cleaned it with alcohol. Drop 1.34 optical fiber matching liquid, because the previous liquid remains, the real value is difficult to achieve 1.34, and the calculation is still calculated according to 1.34; 4) The theoretical maximum value is under the condition that the

polishing plane is parallel to the connection line of the two large air holes. The D-type high birefringence photonic crystal fiber SPR sensor was further used to test the concentration of glucose dissolved. The concentration of glucose solution increases from 0 g/dL to 10 g/dL in steps of 2 g/dL. As the glucose concentration increases, the D-type high birefringence photonic crystal fiber SPR sensor The peak wavelength of the pit of the transmission spectrum will be red-shifted. In the 0 g/dL glucose solution, the SPR resonance wavelength appeared at 578.96 nm, and when the glucose solution concentration was 10 g/dL, the SPR resonance wavelength drifted to 587.49 nm. According to the relationship between the glucose concentration and the peak wavelength of the pit of the transmission spectrum, the average sensitivity is 1.89 nm/(g/dL). The research results show that the D-shaped photonic crystal fiber SPR sensor can be applied to the fields of biology, chemistry and environmental monitoring.

Key words: Photonic crystal fiber; Surface plasmon resonance; Refractive index; Sensor; Side polishing

OCIS codes: 060.5295; 240.6680; 280.1415; 120.4640

Foundation item: National Natural Science Foundation of China (No. 61805051), Natural Science Foundation of Guangxi Province (Nos. 2018JJB170035, 2018AD19071, 2019GXNSFFA245002, 2020JJA170047), Dean Project of Guangxi Key Laboratory of Wireless Broadband Communication and Signal Processing (Nos.GXKL06190118, GXKL06160102,GXKL06180203,GXKL06180104)